

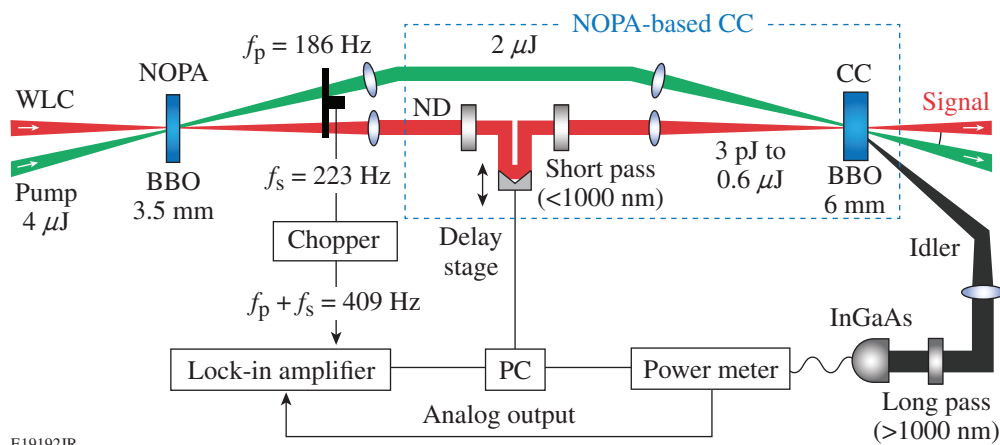
to generate the WLC seed.⁴ The remainder was frequency doubled, producing $4 \mu\text{J}$ for pumping the NOPA, which was a 3.5-mm-thick beta-barium borate (BBO) crystal cut at 21.6° . The NOPA's spectrum and beam profile are shown in Fig. 143.22. The spectrum full width at half maximum (FWHM) was 175 nm (full width at 10% = 210 nm) and the pulse energy was 600 nJ [1.3%-rms (root mean square) pulse to pulse]. The internal noncollinear angle in the BBO crystal was set to 2.3° to maximize the bandwidth and minimize spatiotemporal aberrations induced by the angular-dependent gain of the NOPA.¹¹ The chirp of the WLC and NOPA ($\sim 1300 \text{ fs}^2$) was removed using a standard fused-silica prism compressor to produce 13-fs pulses ($1.07\times$ the Fourier transform limit).

A cross-correlator (CC) based on the NOPA process⁸ was developed to measure the temporal contrast of the uncompressed pulses directly from the NOPA (see Fig. 143.23). The residual NOPA pump pulses ($2 \mu\text{J}$, 523 nm, 250 fs) provide the temporal gate by pumping a second, thicker BBO crystal (6 mm, 27.1°) aligned noncollinearly for maximum bandwidth. Although this pump beam has been partially depleted by the signal in the NOPA ($\sim 50\%$) and will therefore have a non-Gaussian beam profile, this scheme allows for the maximum available pump pulse energy to be used in both the NOPA and CC, maximizing the gain and dynamic range, which would be significantly reduced if the available power were split between the two crystals. The part of the pulse under test (signal) that temporally overlaps the pump is amplified, producing a non-degenerate idler pulse centered at 1250 nm. The signal pulse was sampled over a 350-ps range by varying the delay between the pump and signal and measuring the idler with an InGaAs power meter (Agilent 81624B). One feature of NOPA-based

CC's is that they provide broadband gain and serve as a pre-amplifier for the detection system. When optimally configured, the unsaturated gain is 39 dB with a bandwidth of 150 nm.

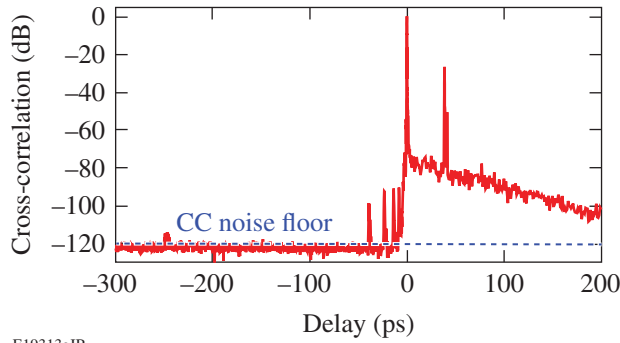
Several techniques were used to minimize noise that would otherwise limit the dynamic range of the CC. Since the signal and idler are non-degenerate, background noise from signal scattering in the CC crystal is reduced by placing a long-pass filter (Schott RG1000, 7 mm thick) before the power meter. Further rejection of scattering and parametric fluorescence from the CC is obtained using a lock-in detection technique as previously demonstrated for second-order autocorrelators.^{12,13} The pump and signal beams are chopped at 186 and 223 Hz, respectively, and the idler component at the sum frequency (409 Hz) from the analog output of the InGaAs power meter is measured using a lock-in amplifier. As a result of the spectral filtering and lock-in detection, all of the available pump and signal energy can be used without saturating the detection system when sampling a low-intensity temporal region of the pulse under test. Calibrated neutral-density filters are inserted in the signal path when sampling the main peak to ensure that the pump pulse is not depleted and, therefore, that the idler power is proportional to the attenuated signal intensity. The CC dynamic range of 120 dB results from the combination of the neutral-density filters (60 dB), the adjustable gain of the InGaAs power meter (40 dB), and the dynamic range of the lock-in detection scheme (20 dB).

A cross-correlation measurement of the uncompressed NOPA pulse is shown in Fig. 143.24. The CC noise floor was determined to be 120 dB below the peak by blocking either the pulse under test or the CC pump. Apart from several discrete



E19192JR

Figure 143.23
Schematic for the NOPA and NOPA-based cross-correlator (CC). PC: personal computer.



E19313aJR

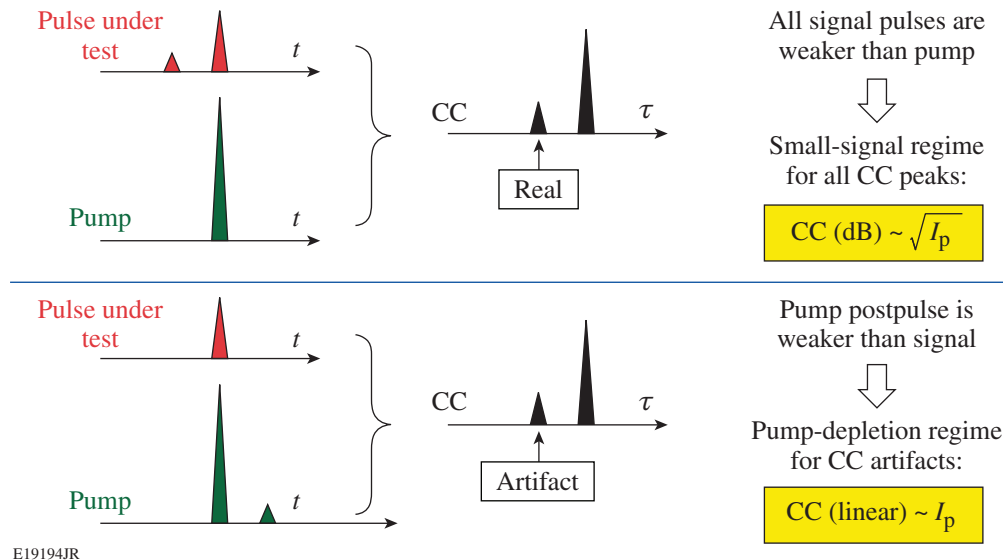
Figure 143.24
Cross-correlation scan.

peaks, the prepulse contrast up to 5 ps before the main peak exceeds the 120-dB CC dynamic range. Note that the width of the uncompressed pulse (~300 fs) has not been deconvolved from these measurements. Therefore, if the peak intensity increase from compressing the pulse from 300 fs to 13 fs is ~13 dB, the compressed pulse contrast exceeds 133 dB.

Determining whether discrete peaks are real prepulses or artifacts caused by gate or pump postpulses is a problem common to all cross-correlators. For a NOPA-based device, however, the main pump pulse provides much more gain for the signal than is provided by lower-intensity pump noise. (The necessary by-product of gain, a parametric fluorescence background, is mitigated using the two-frequency lock-in

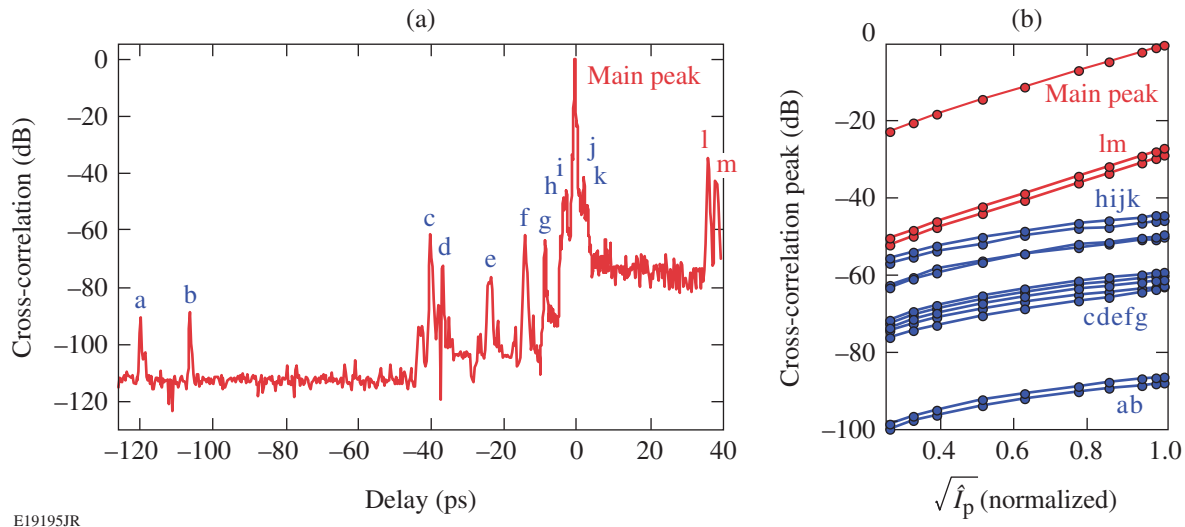
technique.) Moreover, the nature of each peak (whether it is an actual prepulse on the signal-under-test or a measurement artifact created by a postpulse on the pump) can be determined from its scaling with the intensity of the pump (shown schematically in Fig. 143.25). A prepulse on the signal that overlaps with the main pump pulse experiences the maximum small-signal gain; therefore, the CC peak scales exponentially with the pump field.¹⁴ In terms of the pump intensity I_p , the small-signal scaling on a logarithmic scale is $CC(\text{dB}) \sim \sqrt{I_p}$. Alternatively, when a weak pump postpulse overlaps with the main signal peak, the CC gain is much lower. In this “small-pump” limit, the CC peak scales linearly with I_p ; therefore, on a logarithmic plot, $CC(\text{dB}) \sim \log_{10}(I_p)$.

Measurements of the discrete peaks are shown in Fig. 143.26. To emphasize any artifacts, the maximum peak gain of the CC was reduced from 39 to 17 dB by halving the thickness of the CC crystal and increasing the pump spot size. The magnitude of each peak was measured as the pump polarization was rotated using a half-wave plate to vary the amplitude of the phase-matched component of the pump along the crystal axis. The normalized intensity of the pump in terms of the half-wave-plate angle is $\hat{I}_p = \cos^2(2\theta)$. Figure 143.26 shows that all peaks before the main peak scale following the small-pump scaling, $CC(\text{dB}) \sim \log_{10}(\hat{I}_p)$, and are, therefore, artifacts from pump postpulses. Therefore, the prepulse contrast for the uncompressed pulses does not exceed 120 dB.



E19194JR

Figure 143.25
Schematic showing the different intensity scalings to determine whether a cross-correlation peak is caused by a true prepulse before the pulse under test or is an artifact caused by the CC pump postpulse.

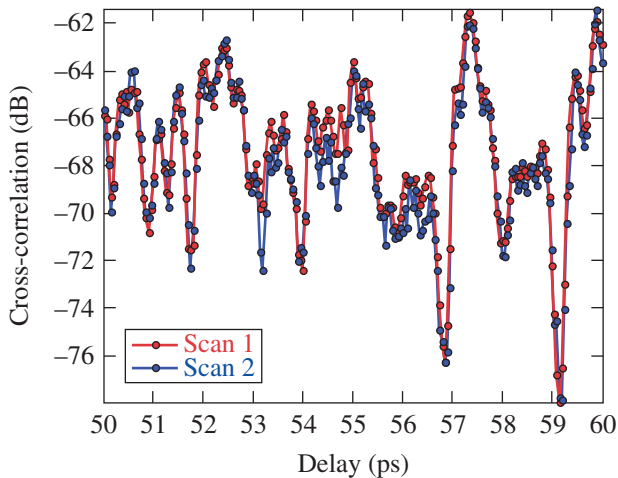


E19195JR

Figure 143.26

(a) Cross-correlation scan taken at reduced CC gain (17 dB) to emphasize artifacts from pump postpulses. (b) Magnitude of each peak for varying normalized pump field ($\sqrt{\hat{I}_p}$). The red curves correspond to the main pulse under test and crystal reflections; the blue curves correspond to artifacts produced by CC pump postpulses.

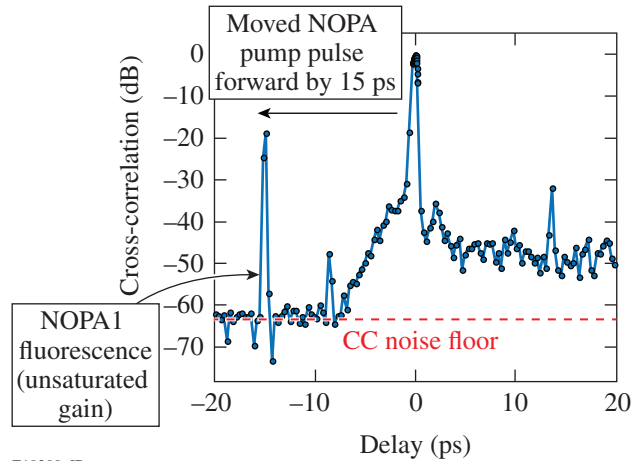
One unexpected feature of the CC measurements is the exponential tail following the main CC peak. The tail has a time constant of 29 ps, an intensity contrast greater than 80 dB, and an energy contrast of 56 dB. It was found that the temporal modulation was repeatable from scan to scan (as shown in Fig. 143.27) and, therefore, is not random noise. Furthermore, very similar scans were measured at a later time when the crystal used to generate the WLC was changed from sapphire to undoped yttrium aluminum garnet. Lastly, Fig. 143.28 shows



E19199JR

Figure 143.27

Section of the postpulse tail, showing the repeatability from scan to scan.



E19200aJR

Figure 143.28

Cross-correlation scan when the NOPA pump pulse was temporally shifted 15 ps before the seed pulse. This shows that a tail is present when there is no gain in the NOPA.

measurements of the unamplified WLC, where the NOPA pump was temporally shifted 15 ps before the seed. These measurements suggest that the tail is not caused by gain in the NOPA. Unfortunately, the dynamic range for the reduced signal level was not sufficiently high (~ 63 dB) to determine whether the tail was also present with the pulse of fluorescence created by the pump pulse. Therefore, it has not been determined if the tail is a result of the WLC process or if it is caused by the CC

optics. Nonetheless, there are typically additional picosecond-pumped NOPA stages before the stretcher, with at least 50 dB of gain, that would suppress the tail to an insignificant level.¹⁵ Furthermore, the temporal contrast after the main pulse is an issue in a CPA system only when self-phase modulations during the amplification of the chirped pulses leads to weaker satellite prepulses.¹⁶

Conclusions

This article reports the first broadband, high-dynamic-range, temporal contrast measurements of a WLC-seeded NOPA. The NOPA-based cross-correlator that was developed for this purpose has a dynamic range, bandwidth, and resolution of 120 dB, 150 nm, and 250 fs, respectively. A simple technique for distinguishing between real prepulses and pump artifacts for any cross-correlator based on parametric amplification has been demonstrated. Measurements over a 350-ps window show that the uncompressed output of the WLC-seeded NOPA has a prepulse contrast that exceeds the 120-dB dynamic range of the cross-correlator up to 5 ps before the main peak. These results, combined with a previous analysis of the WLC-seeded NOPA,¹¹ supports its potential as a front end for ultra-intense OPCPA systems.

ACKNOWLEDGMENT

This material is based upon work supported by the Department of Energy National Nuclear Security Administration under Award Number DE-NA0001944, the University of Rochester, and the New York State Energy Research and Development Authority. The support of DOE does not constitute an endorsement by DOE of the views expressed in this article.

REFERENCES

1. Y. Tang *et al.*, *Opt. Lett.* **33**, 2386 (2008).
2. V. V. Lozhkarev *et al.*, *Opt. Express* **14**, 446 (2006).
3. V. V. Lozhkarev *et al.*, *Laser Phys.* **15**, 1319 (2005).
4. J. Bromage, C. Dorrer, and J. D. Zuegel, in *Advances in Optical Materials*, OSA Technical Digest (CD) (Optical Society of America, Washington, DC, 2011), Paper JWC2.
5. M. K. Reed *et al.*, *J. Opt. Soc. Am. B* **12**, 2229 (1995).
6. T. Wilhelm, J. Piel, and E. Riedle, *Opt. Lett.* **22**, 1494 (1997).
7. A. Shirakawa *et al.*, *Appl. Phys. Lett.* **74**, 2268 (1999).
8. E. J. Divall and I. N. Ross, *Opt. Lett.* **29**, 2273 (2004).
9. T. V. Andersen *et al.*, *Opt. Express* **14**, 4765 (2006).
10. C. Schriever *et al.*, *Opt. Lett.* **33**, 192 (2008).
11. J. Bromage, C. Dorrer, and J. D. Zuegel, *Opt. Lett.* **35**, 2251 (2010).
12. A. Braun *et al.*, *Opt. Lett.* **20**, 1889 (1995).
13. P. F. Curley *et al.*, *Opt. Commun.* **120**, 71 (1995).
14. G. Cerullo and S. De Silvestri, *Rev. Sci. Instrum.* **74**, 1 (2003).
15. J. Bromage, C. Dorrer, M. Millecchia, J. Bunkenburg, R. Jungquist, and J. D. Zuegel, in *Conference on Lasers and Electro-Optics 2012*, OSA Technical Digest (online) (Optical Society of America, 2012), Paper CTh1N.7.
16. D. N. Schimpf *et al.*, *Opt. Express* **16**, 10,664 (2008).